Plant Biotechnology Journal
Open Access

Plant Biotechnology Journal (2025) **23**, pp. 2095–2109 doi: 10.1111/pbi.70040

RPT: An integrated root phenotyping toolbox for segmenting and quantifying root system architecture

Jiawei Shi[1,†], Shangyuan Xie[1,†], Weikun Li[1,†], Xin Wang[1,2], Jianglin Wang[1], Yunyu Chen[1], Yongyue Chang[1], Qiaojun Lou[2,3,*] and Wanneng Yang[1,*]

[1]*National Key Laboratory of Crop Genetic Improvement and National Center of Plant Gene Research (Wuhan), Hubei Hongshan Laboratory, Huazhong Agricultural University, Wuhan, China*

[2]*Shanghai Agrobiological Gene Center, Shanghai, China*

[3]*Zhejiang Crop Genebank, Zhejiang Academy of Agricultural Sciences, Hangzhou, China*

Received 27 December 2024;
revised 17 February 2025;
accepted 19 February 2025.
**Correspondence* (Tel +86-27-8728-2120; fax +86-27-8728-1536; email ywn@mail.hzau.edu.cn (W.Y.); Tel/fax +86-571-8605-8265; email lqj@sagc.org.cn (Q.L.))
[†]These authors contributed equally to this article.

Keywords: deep learning, high-throughput phenotyping platform, rice drought resistance, root phenotyping, root system architecture.

Summary

The dissection of genetic architecture for rice root system is largely dependent on phenotyping techniques, and high-throughput root phenotyping poses a great challenge. In this study, we established a cost-effective root phenotyping platform capable of analysing 1680 root samples within 2 h. To efficiently process a large number of root images, we developed the root phenotyping toolbox (RPT) with an enhanced SegFormer algorithm and used it for root segmentation and root phenotypic traits. Based on this root phenotyping platform and RPT, we screened 18 candidate (quantitative trait loci) QTL regions from 219 rice recombinant inbred lines under drought stress and validated the drought-resistant functions of gene *OsIAA8* identified from these QTL regions. This study confirmed that RPT exhibited a great application potential for processing images with various sources and for mining stress-resistance genes of rice cultivars. Our developed root phenotyping platform and RPT software significantly improved high-throughput root phenotyping efficiency, allowing for large-scale root trait analysis, which will promote the genetic architecture improvement of drought-resistant cultivars and crop breeding research in the future.

Introduction

Rice holds a crucial position in the global food system, and as a staple, it supports nearly half of the global population (Zhang, 2007). Rice cultivation has a high demand on the growth environment, requiring sufficient water. However, with the exacerbation of climate change and water scarcity, rice production is faced with tremendous challenges (Vogel *et al*., 2019). In addition, soil salinization sharply reduces the arable land area of rice cultivation (Mukhopadhyay *et al*., 2021), directly affecting the growth and development of rice root systems, which play a key role in water and nutrient absorption (Santos-Medellín *et al*., 2021). In terms of rice drought resistance, rice is primarily categorized into four types: drought avoidance, drought tolerance, drought recovery and drought escape (Luo *et al*., 2019). Achieving drought avoidance requires a strong and well-developed root system. Robust root systems of crops can absorb water from deep soil layers, enabling crops to grow normally even under drought stress (Ahmadi *et al*., 2014). Therefore, it is essential to explore the strategies to improve rice root phenotypes and enhance rice drought tolerance for ensuring rice yield and global food security (Meng *et al*., 2019).

Rice root traits are predominantly controlled by multiple genes, and many genes and quantitative trait loci (QTL) related to the rice root system have already been identified. In an early study on root trait QTL mapping of a japonica-japonica hybrid doubled haploid (DH) line, 18 additive and 18 epistatic QTLs of seven traits, including maximum root length, have been detected (Mu, 2003). Gene *DRO1* has been found to enhance deep root development and rice drought resistance by influencing root system angle in a recombinant inbred line rice derived from crossing the indica variety 'IR64' and the japonica upland variety 'Kinandang Patong' (Uga *et al*., 2011). Overexpression of *OsNAC5* can increase rice root diameter, thereby enhancing rice drought resistance and yield (Jeong *et al*., 2013). A genome-wide association study (GWAS) has identified 110 significant association loci and 11 genes related to root traits, including *DRO1*, *WOX11* and *OsPID*, from 529 natural rice populations under drought stress (Li *et al*., 2017).

Currently, root shovelling is the primary method for investigating root phenotypes, but this method is time-consuming and labour-intensive (Atkinson *et al*., 2019), making high-throughput root phenotyping difficult. Although there are some automated root excavation and washing methods (Trachsel *et al*., 2011), these methods disrupt the root topology, causing irreversible damage to the root system. The computed tomography (CT) (Haling *et al*., 2013) and magnetic resonance imaging (MRI) (van Dusschoten *et al*., 2016) are major methods for root phenotyping in soil environments (Li *et al*., 2022), but the high cost and image reconstruction difficulty limit their large-scale application (Metzner *et al*., 2015). In contrast, the rhizobox method, as a widely recognized method for root phenotyping, allows non-destructive dynamic observation of root growth in inclined boxes (Nagel *et al*., 2012). Compared to hydroponics (Chen *et al*., 2011), the agar method (Nagel *et al*., 2020) and aeroponics (Selvaraj *et al*., 2019), the rhizobox method can better reflect the true performance of roots in soil environments, making

it a desirable option for high-throughput root phenotype research.

Although rhizobox-based root phenotyping platforms offer significant advantages, such as enabling clear two-dimensional visualization of roots due to their structural design and facilitating high-throughput manufacturing, the substantial cost associated with producing large quantities of rhizoboxes remains a limiting factor. This high cost hinders the full realization of high-throughput capabilities in large-scale applications. Additionally, processing large amounts of image data generated by high-throughput root phenotyping systems and quickly extracting phenotype traits pose a great challenges. For obtaining root phenotypes from clean non-soil backgrounds, open-source softwares such as WinRHIZO (Arsenault *et al.*, 1995) and IJ_Rhizo (Pierret *et al.*, 2013) are recognized as effective tools. For extracting root traits from complex soil backgrounds, the extensively used softwares include WinRHIZO TRON (Regent Instruments, Quebec, Canada), DART (Le Bot *et al.*, 2010), RootNAV (Pound *et al.*, 2013) and others, but root manual sketchings and large volume of image processing are required, which is time-consuming. Moreover, these software programs are unable to inpaint broken roots, affecting the accuracy of trait calculations. Thus, it is essential to develop a tool for rapid root image segmentation in soil backgrounds along with the capability to inpaint broken roots.

The rapid development of deep learning offers a potential solution to root segmentation (Kamilaris and Prenafeta-Boldú, 2018). Some semantic segmentation methods to segment roots in soil have been documented (Bosilj *et al.*, 2020; Luo *et al.*, 2024; Milioto *et al.*, 2018). Current root phenotyping methods face a critical gap in integrating root segmentation with downstream trait extraction, often requiring additional software or manual intervention, which is time-consuming and error-prone. To address this, a unified, user-friendly and extensible root image analysis tool is urgently needed to streamline the entire workflow—from image preprocessing to automated trait extraction (e.g. root length, diameter, spatial distribution). Such a tool would enhance efficiency, accuracy and scalability while allowing customization for diverse crops and research needs.

In this study, we developed a high-throughput root phenotyping platform containing automated photography equipment, which could complete the imaging of 1680 rhizoboxes within 2 h, enabling dynamic, non-destructive observation of crop roots in the seedling stage. Additionally, we developed a root phenotyping toolbox (RPT), integrating enhanced root segmentation, model training and trait extraction functions, which can also process images captured by other root phenotyping platforms. Our root phenotyping platform and RPT were demonstrated to effectively dissect drought-related genetic architecture in rice roots. Our findings provide a valuable reference for improving rice root system architecture and breeding drought-resistant rice cultivars.

Results

Enhanced SegFormer network for root segmentation

High-throughput platforms generate large amounts of data, making efficient processing a challenge. Fine root segmentation, especially for roots with diameters of about 5 pixels in rice root images, is particularly difficult. Deep learning models typically down-sample input images to generate feature maps, resulting in a loss of shallow-layer details, which lowers segmentation accuracy, especially at root edges. While SegFormer's transformer-based architecture excels in capturing global context, it still struggles with fine root edge details. To address this, we integrated an edge attention module (EAM) into SegFormer to improve the effect of segmentation (Figure 1a). The EAM is designed with the aim of capturing rich primary features and improving edge segmentation accuracy. The EAM module is composed of four CBR modules (Convolutional layers, Batch Normalization [BN]), and ReLU activation) and a convolutional block attention mechanism module (CBAM). At each convolutional layer of the 4 CBR modules, the dilation rate and padding size of the convolution kernels are set as 1/1/2/5, respectively, with a kernel number of 16/64/128/256. To downsample the data and extract primary features, the convolution operation stride is set as 2 in the first two convolution operations and as 1 in the last two convolution operations.

The CBAM module consists of a channel attention module and a spatial attention module. Firstly, the images are processed by the four CBR modules to generate a feature map rich in contextual information. Subsequently, the generated feature map is input into the CBAM module where the feature channels are filtered by the channel attention module to obtain the important feature channels at a compression ratio of 16. Finally, the feature map is input to the spatial attention module to identify key regions from the feature map.

We assessed the performance of various root segmentation models, including traditional models (such as DeepLabV3+ [Chen *et al.*, 2018], Pspnet [Zhao *et al.*, 2017], Segnet [Badrinarayanan *et al.*, 2017] and U-net [Ronneberger *et al.*, 2015]), the baseline SegFormer model and our proposed enhanced ESegFormer model. Model evaluation indicators included mean dice coefficient (mDice), mean intersection over union (mIoU), mean accuracy (mAcc), processing time and parameter number. A detailed model performance comparison is presented in Table 1.

As shown in Table 1, our proposed ESegFormer model outperforms all other models in multiple evaluation metrics. Notably, our model achieves the highest mDice coefficient (0.8392) and mIoU score (0.7555). In addition, the ESegFormer model also exhibits a higher work efficiency, with a processing time of an image per 7.53 s, and requires lower computational resources, with a parameter number of 28 525 796. Figure 1b further illustrates the relationship between parameter number and mDice index for each model. The ESegFormer model achieves the highest mDice value while maintaining a moderate parameter count, demonstrating an effective balance between performance and computational cost. Figure 1c visualizes the normalized performance of each model on various test datasets, enabling a comprehensive comparison of root segmentation performance among various models. ESegFormer consistently displays higher segmentation accuracy than other models on a majority of test datasets in most scenarios.

In short, the ESegFormer model establishes a new criterion for root segmentation, exhibiting high accuracy and computational efficiency. Its high work efficiency makes it an ideal option for mining rice drought-resistant genes.

Root trait extraction using RPT

The RPT software developed using Python provides an interactive graphical user interface (GUI) (Figure 2a), allowing users to

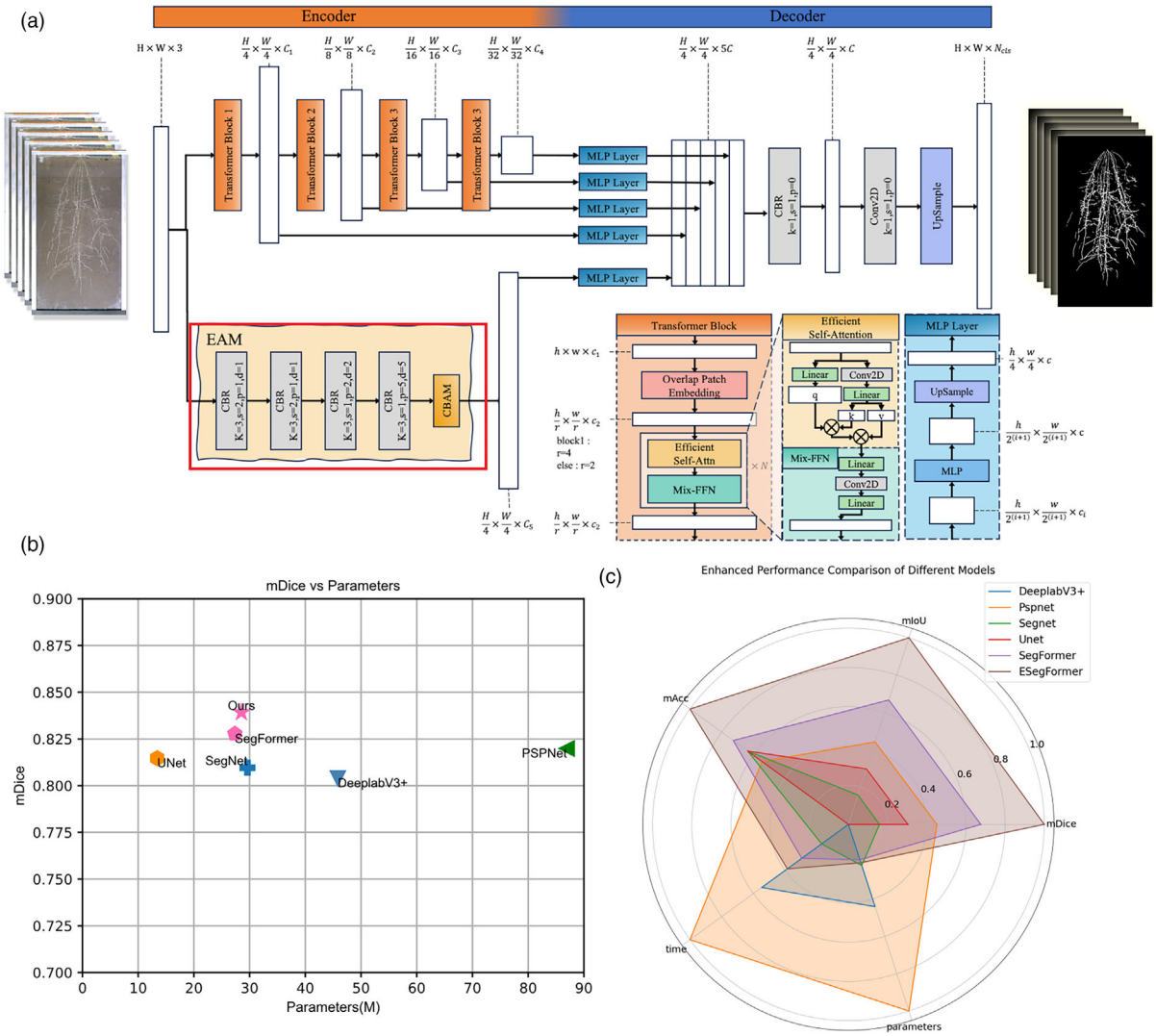

Figure 1 ESegFormer model architecture and comparison of different segmentation models. (a) The ESegFormer model developed based on the SegFormer model integrates the edge attention module (EAM) to enhance its performance. (b) Performance indicators of various segmentation models. (c) Satellite view of the six segmentation models across different test samples. All model parameters are normalized to facilitate intuitive comparison.

Table 1 Performance comparison of different models

Model	mDice	mIoU	mAcc	Time (s)	Parameters
DeeplabV3+	0.8040	0.7168	0.9936	7.57	45 834 226
Pspnet	0.8199	0.7339	0.9942	10.56	86 946 404
Segnet	0.8096	0.7229	0.9943	5.66	29 608 130
Unet	0.8147	0.7283	0.9943	4.74	13 404 354
SegFormer	0.8278	0.7426	0.9944	6.94	27 349 698
ESegFormer	0.8392	0.7555	0.9947	7.53	28 525 796

perform root image segmentation, inpainting and trait extraction. The original image-based root segmentation can generate binary root images in which the segmented roots tend to be discontinuous due to soil shielding. The inpainting function of RPT can address this discontinuity by reconstructing partial roots, thus presenting a more complete root system. After inpainting, noise removal is performed on the enhanced images, hence increasing trait extraction accuracy. The RPT can extract multiple root traits simultaneously, such as root area, convex hull area, length, depth, average diameter, width-to-depth ratio, density, root angles and some derivative traits, and it segments roots in images into upper and lower layers. Detailed trait information is shown in the Table S1.

To investigate the measurement accuracy of RPT, we compared eight traits extracted by RPT and RhizoVision Explorer software, including area, convex hull area, depth, width, length, average diameter, width/depth ratio and density (Seethepalli *et al.*, 2021). RhizoVision Explorer is widely recognized for its accuracy in root trait measurements. The comparison reveals a strong correlation ($R^2 = 0.98$–0.99) between the calculation results of the two root extraction tools, confirming the accuracy of the RPT trait calculation. This further demonstrates the reliability and robustness of the RPT approach in root trait analysis (Figure 2b).

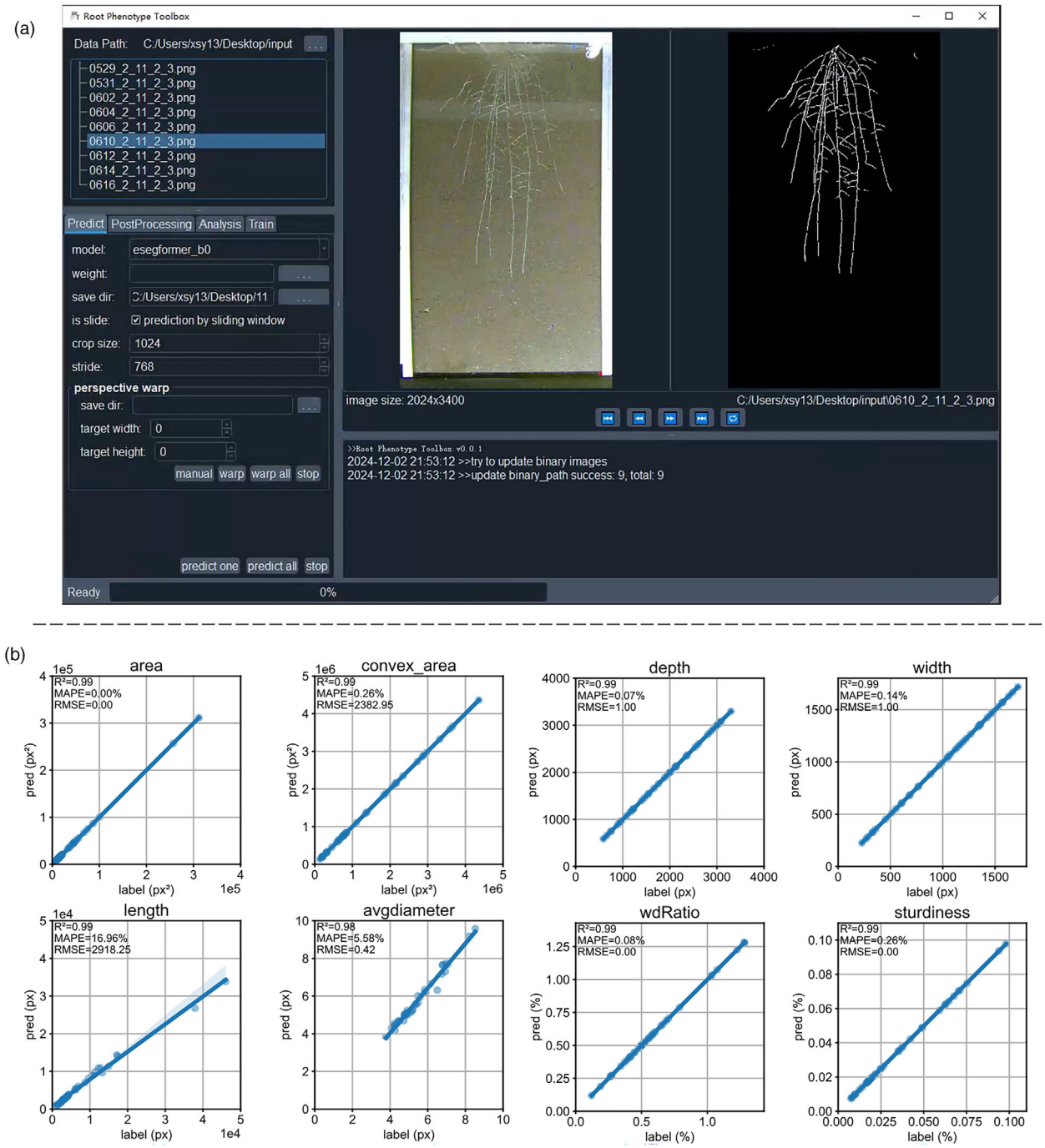

Figure 2 GUI and the regression scatter plot of root traits, respectively, by RPT and RhizoVision Explorers. (a) GUI of RPT Software. (b) Regression scatter plot. In the scatter plot, the label (X axis) represents the results calculated by RhizoVision Explorer, while the pred (Y axis) indicates the predicted results calculated by RPT. RPT, root phenotyping toolbox; GUI, graphical user interface.

Rice drought resistance test using high-throughput root phenotyping platform and RPT

The drought experiments of 219 recombinant inbred lines (RILs) were performed on the high-throughput root phenotyping platform. Using the high-throughput root phenotyping platform, red-green-blue (RGB) images of 42 root traits were captured at 16 different time points after sowing. The effectiveness of the root inpainting model was evaluated through a comparative analysis. The comparison revealed significant differences in root area, root length and three traits based on the root depth ratio in rhizoboxes, including mass_1_L_Ratio (root depth ratio at the upper layer and lower layer [layer 1, 900 pixels: below]), mass_2_L_Ratio (layer 2, 1800 pixels: below) and mass_3_L_Ratio (layer 3, 2700 pixel: below) between the well-watered group (WW) and the drought-stressed (DS) group (irrigation cessation on day 18 post sowing), while the width trait exhibited no significant difference between the two groups (Figure 3a and Table S2).

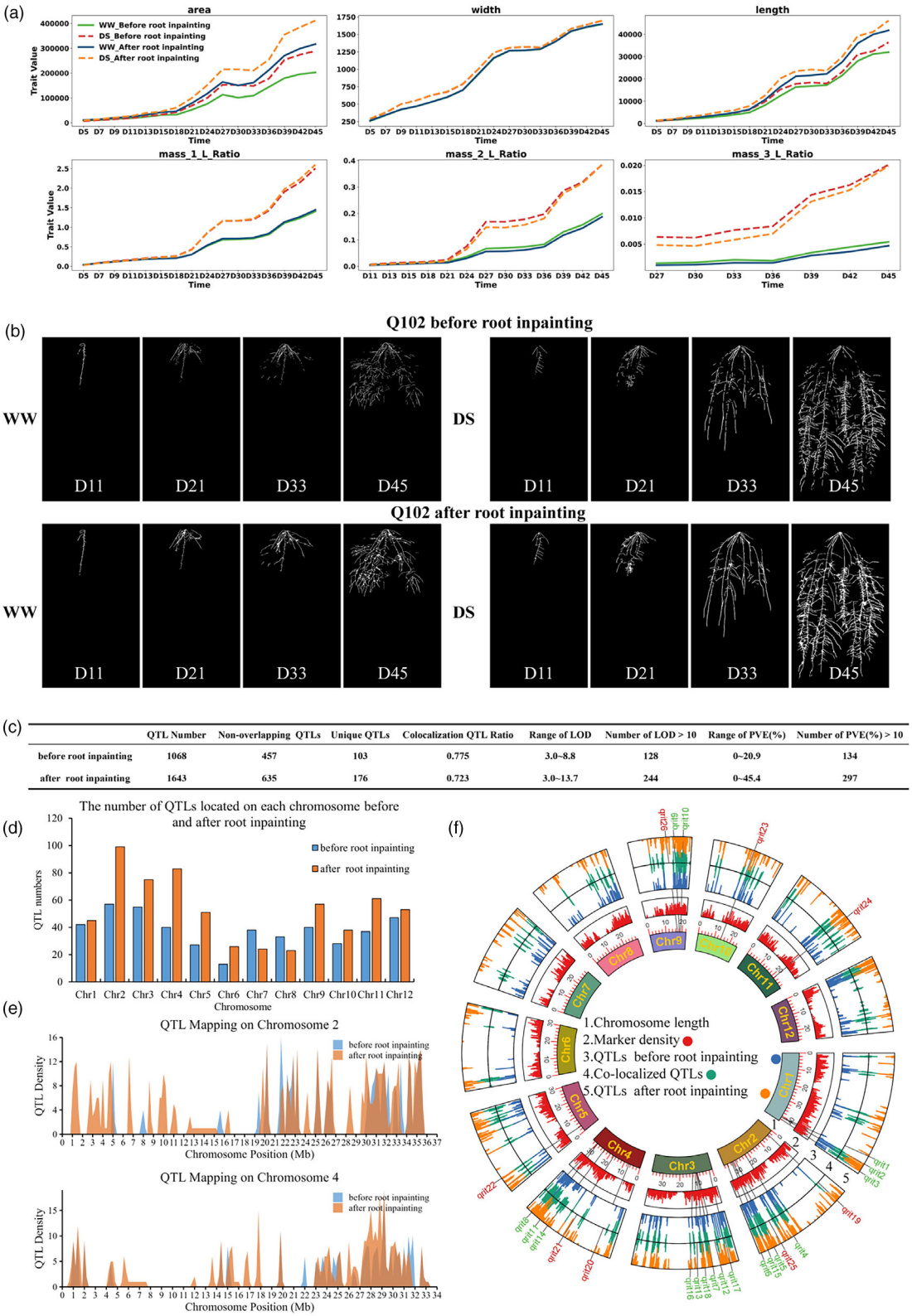

Figure 3 Partial root image traits and QTL mapping results before and after root inpainting under water and drought conditions. (a) Six image-based root traits before and after root inpainting under water and drought conditions through a 45-day experimental period. (b) Root segmentation images of the Q102 line at different time points before and after root inpainting under water and drought conditions. (c) QTL mapping results before and after root inpainting. (d) Number of QTLs located on different chromosomes before and after root inpainting. (e) The QTL distribution on chromosome 2 and chromosome 4 before and after root inpainting. (f) QTL mapping results of all traits. (1) Chromosome length, (2) Marker density, (3) QTLs before root inpainting, (4) Co-localized QTLs, and (5) QTLs after root inpainting.

We also carried out root inpainting on the obtained root segmentation images. After root inpainting (image restoration), the trait values of the root area and length were significantly increased, while the trait values of width and mass_1_L_Ratio displayed no obvious differences before and after root inpainting. In contrast, mass_2_L_Ratio and mass_3_L_Ratio trait values were slightly lower than those before root inpainting. The root segmented image inpainting resulted in the most significant increase in root length between the WW group and DS group in the Q102 line (Figure 3b). These results indicated that root inpainting increased the root length in the middle part and lower part of the rhizobox.

Further, we combined root trait image data with previously reported genomic sequencing data to map quantitative trait loci (QTLs) (Table S3). The results showed that root inpainting significantly increased the number of QTLs by approximately 53.84%, including 176 unique QTLs (Figure 3c and Table S4). After inpainting, the detected QTLs exhibited a broader range of logarithm of odds (LOD) scores, with the maximum LOD increasing from 8.8 before inpainting to 13.7. Furthermore, the mapped QTLs post inpainting showed a higher phenotypic variance explained (PVE), with the maximum increasing from 20.9% before restoration to 45.4% after inpainting. After root inpainting, the number of mapped QTLs increased on nearly all chromosomes (except chromosomes 7 and 8), with chromosome 2 exhibiting the largest number (99) of mapped QTLs (Figure 3d). In Figure 3e, we illustrate the distribution of QTL mapping on the two chromosomes (Chromosome 2 and Chromosome 4) that showed the most pronounced differences before and after root inpainting. The 18 candidate QTLs (qrit1-qrit18) that were repeatedly first mapped across multiple traits were selected from the mapped QTLs before root inpainting (Table S4). These 18 selected candidate QTLs were also re-mapped to root image traits after root inpainting, confirming the reliability of inpainting. By aligning the physical maps of IRAT109 and Nipponbare (Nip) lines, a 100 kb upstream and downstream region of each candidate QTL was determined. By screening drought-related genes within the candidate QTL regions based on MBKbase (https://www.mbkbase.org/) and the China Rice Data Center (https://www.ricedata.cn/), 12 genes associated with drought resistance in rice were identified. Of these 12 genes, *OsSDIR1* has been reported to enhance drought tolerance under drought stress (Matsuda *et al*., 2016); *OsPYL6* regulates rice development and drought tolerance (Santosh Kumar *et al*., 2021); and *OsABAR1* improves drought tolerance in an ABA-dependent manner (Zheng *et al*., 2020); and the remaining nine drought-related genes included *OsGS1* (Singh and Ghosh, 2013), *OsDHODH1* (Liu *et al*., 2009), *OsNAP* (Chen *et al*., 2014), *Osr40c1* (Sahid *et al*., 2023), *CYP96B5* (Zhang *et al*., 2020), *OsDSS1* (Tamiru *et al*., 2015), *OsABCG5* (Matsuda *et al*., 2016), *OsMAPK5* (Xiong and Yang, 2003) and *OsRCI2-5* (Li *et al*., 2014). Additionally, the extra 176 unique QTLs were mapped after root inpainting, from which eight candidate QTLs with high PVE or LOD values were selected. From these eight QTL regions, two reported drought resistance-related genes, *OsABA8ox1* and *OsbZIP72*, were identified (Baoxiang *et al*., 2021; Shi *et al*., 2015). The Circos plot displayed chromosome length, marker density and the QTL mapping and co-localization before and after root inpainting (Figure 3f). Based on root phenotypic data, multiple mapped QTLs were found to be primarily located at the ends of the chromosomes. The candidate QTLs were mainly concentrated on chromosomes 1, 2, 3, 4 and 9. After root inpainting, three extra candidate QTLs were identified on chromosomes 5, 10 and 11.

Finally, to further validate the reliability of the localization results, candidate gene *OsIAA8* (LOC_Os02g49160) associated with root development and stress resistance in rice was identified from the candidate QTL qrit5 region. The rhizobox platform was utilized to cultivate the *OsIAA8*-overexpressing line (IAA8OE) and its wild-type control line (Nip), and pot experiments were conducted to validate rhizobox experiment results. Under well-watered (WW) conditions, IAA8OE plants showed higher shallow root biomass than Nip plants, while under drought–stress (DS) conditions, IAA8OE exhibited a larger proportion of deep roots than Nip (Figure 4a and Table S5). Under WW conditions, IAA8OE plants displayed a higher root biomass at the shallow soil layer, whereas under DS conditions, root biomass at the deep soil layer was increased, indicating that plants might increase root depth to access additional water and sustain growth in response to stress. This was validated by pot experiment results that after 10days of drought stress, Nip plants exhibited significant leaf curling, while IAA8OE plants maintained fully extended leaves (Figure 4b). Under drought stress, total projection area (TPA), green projection area (GPA), total projected area/bounding rectangle area (TBR), and other image-based trait values significantly decreased in Nip plants, but they were only slightly decreased in IAA8OE plants. These results indicated that IAA8OE plants enhanced drought resistance potentially by increasing root biomass at the deep soil layer to maintain normal growth under drought conditions.

In short, the high-throughput root phenotyping platform enables the extraction of a large number of time-series root image traits, facilitating dynamic phenotypic observation of root response to drought stress. Our data showed that drought treatment promoted root growth at deep soil layers. The application of the root inpainting model further increased the accuracy of root image traits, as evidenced by increased root area and length. Root inpainting led to an increase in the number of mapped QTLs of 53.84%, higher LOD scores and PVE values. Overall, the high-throughput root phenotyping platform significantly contributes to root phenotyping, and the application of root image traits increases the identification accuracy of reported drought-related genes, aiding in the discovery of new drought-resistance candidate genes. The root image inpainting model constructed in this study further improves the accuracy of root trait image data and facilitates the exploration of novel drought-related loci. Additionally, both rhizobox and pot experiments on *OsIAA8*-overexpressing lines demonstrated that the high-throughput root phenotyping platform could effectively identify drought-resistant genes through root phenotyping.

Discussion

Currently, root phenotyping remains a great challenge. The invisibility of roots in the soil poses a significant barrier to dynamically observing root systems in a non-destructive manner. High-throughput phenotyping is essential (Yang *et al*., 2020), and it can provide vital data for crop improvement technologies such as genome-wide association studies (GWAS) and genomic selection (GS) (Bolger *et al*., 2017; Cobb *et al*., 2013). High-throughput phenotyping of root traits can deepen our understanding of root system architecture and its relationship with plant performance under various environmental conditions.

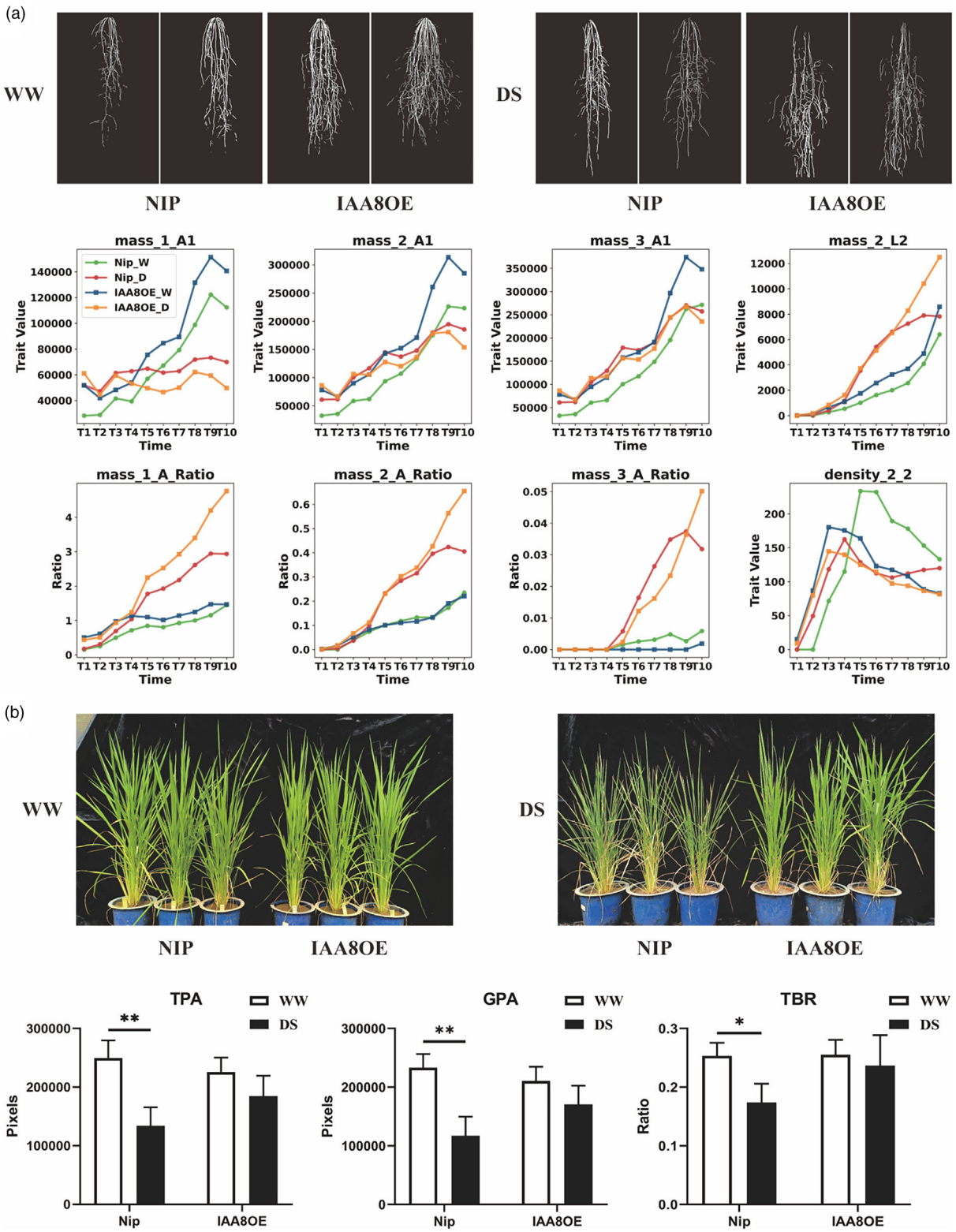

Figure 4 Rhizobox and pot experiments of drought resistance of OsIAA8-overexpressing (IAA80E) and Nip materials. (a) Dynamic changes in root phenotypes and root image traits of IAA8OE and Nip materials. (b) Phenotypes and image traits of the above-soil parts of IAA8OE and Nip materials on day10 post drought treatment. Asterisks indicate significant differences as determined by a one-tailed Student's *t*-test: '*' and '**' represent significance at the $P < 0.05$ and $P < 0.01$ levels, respectively.

However, achieving a balance between throughput and cost is a critical consideration in the development of root phenotyping platforms. Traditional methods such as CT and magnetic resonance imaging (MRI) enable non-destructive, three-dimensional root phenotyping but are often prohibitively expensive for large-scale breeding programmes. In contrast, our

platform addresses this challenge by offering a cost-effective solution that does not compromise on throughput or accuracy.

Our platform leverages rhizobox-based imaging techniques, which provide a non-destructive and economical alternative for high-throughput root phenotyping. By utilizing two-dimensional images, our platform achieves a significant reduction in cost compared to 3D imaging technologies while maintaining high throughput. This balance is achieved by integrating advanced image processing algorithms with a scalable hardware design that is as simple structured as possible, which minimizes operational expenses without sacrificing data quality. Such as the hardware platform designed in this study, such as the rhizobox, is composed of stainless steel, toughened glass, and screws, which are strong enough and cheap to process. Only one set of camera and motion module is needed to meet the high throughput shooting. The cost-effectiveness of our platform makes it particularly suitable for large-scale breeding studies, where the ability to phenotype hundreds or thousands of plants efficiently is essential. Notably, the existing platforms such as GROWSCREEN-Rhizo and GLO-Roots (Rellán-Álvarez *et al.*, 2015) have demonstrated successful applications in soil root system architecture (RSA) studies. Although GROWSCREEN-Rhizo offers potent population investigation capability, its high cost restricts its application. In spite of its greater affordability, GLO-Roots exhibits limited container size and application scenarios. Many low-cost observation containers have been developed (Bontpart *et al.*, 2020), but their high-throughput scalability is far from satisfactory.

This study demonstrates the feasibility and applicability of our platform and algorithm for rice phenotyping, and their application can be further extended to other species such as cotton and wheat (Figure 5a), highlighting the adaptability and scalability of our platform and RPT. The RPT has demonstrated robust performance in phenotyping root images from various platforms and laboratories, highlighting its robustness and compatibility (Figure 5b–d). Although the proposed ESegformer model was not trained on these specific datasets, it adapts well to new data without requiring dataset-specific training, exhibiting a high degree of universality. However, its performance may be suboptimal when applied to images with significant feature differences. To address this limitation, we fine-tuned the ESegformer model by introducing a small number of labelled images from other high-throughput platforms, successfully adapting it to new datasets (Figure 5e). This significantly enhances the model's adaptability, enabling its application to diverse root phenotyping systems with minimal additional labelled data, thereby improving the flexibility and efficiency of root trait analysis. The RPT allows the user to modify the source code to optimize functions such as image cleaning and trait extraction for more accurate and efficient root phenotyping.

The high-throughput root phenotyping platform enables dynamic observation of root responses to drought stress by capturing time-series root image traits. Under drought stress, rice typically exhibits increased root length and area. By employing the root inpainting model integrated into our RPT software, a unique and innovative feature of our platform, we obtained clearer and more accurate data on the changes in deep root structure in response to drought stress. This advanced functionality enables the reconstruction of incomplete or obscured root segments, significantly enhancing the reliability and precision of root trait analysis under challenging imaging conditions. Furthermore, the inpainting of root traits helped identify a larger number of QTLs with higher LOD scores and LOD values. Validation experiments conducted in both rhizobox and pot setups demonstrated that OsIAA8-overexpressing lines exhibited more drought-resistant phenotypes compared to control groups. This further supports the utility of the root phenotyping platform in identifying drought-resistant genes in rice.

Further improvements in the scalability, accuracy and versatility of root phenotyping systems are of great significance. Therefore, future studies are suggested to optimize deep learning models to ensure that they can handle a wider variety of root images and environmental variables. Additionally, the development of cost-effective and scalable systems for root phenotyping will be essential to bridge the gap between laboratory research and field applications. By improving the affordability and accessibility of high-throughput phenotyping systems, these systems are expected to be applied to a broader range so as to promote the breeding of crops with improved root traits such as enhanced yield and drought resistance.

Integrating advanced imaging techniques such as hyperspectral imaging with deep learning algorithms will allow for a more comprehensive understanding of root systems, thus leading to the identification of new phenotypic traits related to root physiological features, especially under abiotic stresses. Ultimately, the development of robust, cost-effective root phenotyping systems is key to accelerating crop breeding progression and addressing the challenges posed by climate change and global food security.

Materials and methods

Materials

The stable recombinant inbred lines (RILs) were constructed with 'IRAT109' and 'Hanhui 15' as parents, and the *OsIAA8*-overexpressing material was genetically modified with Nip as the background. 'IRAT109', as an African japonica rice variety, is characterized by its high-temperature tolerance, well-developed root system and strong drought avoidance trait (Luo *et al.*, 2019). 'HanHui 15' is a restorer line of water-saving and drought-resistant rice (WDR), known for its strong drought resistance, high disease resistance and high-temperature tolerance. The RILs were developed using a single seed descent method for eight generations. A total of 1490 individuals of the RILs were re-sequenced; more than 1 000 000 SNPs of the population were called; and a high-density genetic map was co atrous separable convonstructed. Totally, 217 lines with consistent heading periods from the re-sequenced population were used for subsequent experiments.

Drought resistance evaluation of rice populations and mutants

The first-year drought resistance evaluation experiment of the rice population was performed to obtain candidate drought-resistant QTLs using the high-throughput root phenotyping platform since 7 September 2022, at Huazhong Agricultural University (Wuhan, China). The rice seeds were soaked, germinated and sown in rhizoboxes using tweezers, with two seeds per rhizobox. There were at least six rhizoboxes for each material, with three for the control group and the other three for the drought treatment group. A total of 1512 rhizoboxes were used, and they were thoroughly watered immediately after sowing. Excessive rice seedlings were removed 3 days after sowing to ensure only one seedling in each rhizobox. The root images were captured every

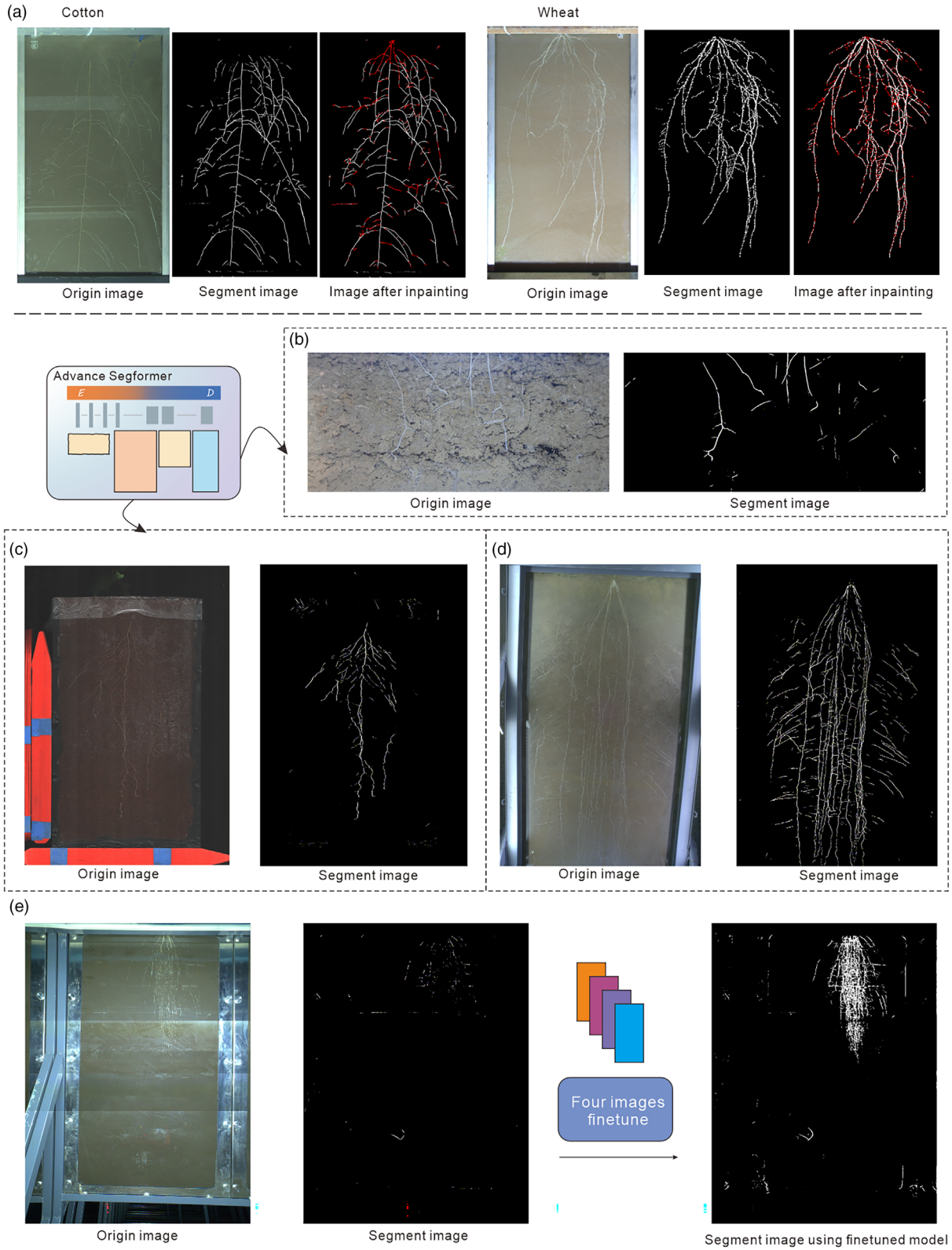

Figure 5 Model Generalization Test. (a) The images of wheat and cotton roots captured using the root phenotyping platform and their segmentation and inpainting by RPT. The red region represents the inpainted root portions. (b) Segmentation of the root system image of *Cichorium intybus* line. Image source: the University of Copenhagen (Smith *et al.*, 2020). (c) Sesame root system image segmentation. Image source: Texas A&M University (Peeples *et al.*, 2023). (d) Wheat root system image segmentation. Image source: Crop Phenotyping Platform, Henan University. (e) Images collected from the large rhizobox platform (left panel), root segmentation results (middle panel) by RPT and root segmentation results (right panel) by the ESegFormer model fine-tuned based on four labelled images.

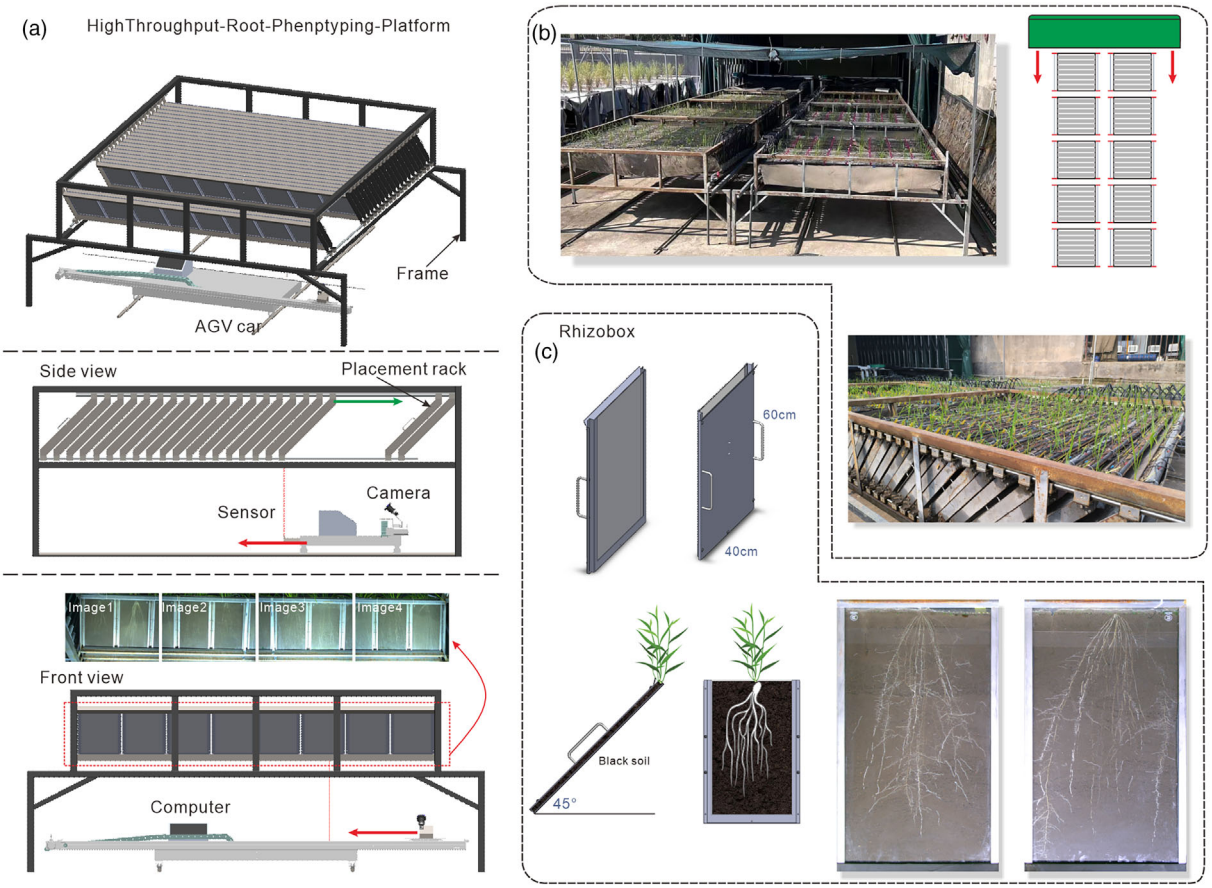

Figure 6 Overview of high-through root phenotyping platform. (a) 3D model of the overall platform framework with automated guided vehicle (AGV) and its tracks. Images captured by the platform, the side view and front view are presented below the framework. (b) On-site images of overall platform in operation. (c) Rhizobox structural diagram (left), images of rice seedling in rhizoboxes (upper right), and root images of different materials (lower right).

2 days from day 5 (D5) after sowing and every 3 days from day 15. The seedlings were drip irrigated in the morning and evening, and the water valve was not turned off until water dripped from the bottom of the rhizobox to ensure thorough irrigation. From day 20 after sowing, irrigation was stopped in the drought stress group, while it was continued in the control group.

To verify the drought resistance of gene *OsIAA8* in candidate QTLs, the second-year rhizobox experiment was conducted from 19 May 2023, at Huazhong Agricultural University (Wuhan city, China). The *OsIAA8*-overexpressing seeds were soaked in a hygromycin solution (at hygromycin/water ratio of 1:1000) to obtain *OsIAA8*-overexpressing seedlings, and the control group was soaked only in water. Then we transplanted the seedlings to rhizoboxes on 24 May 2023, and captured the root images every 3 days from 3 June to 30 June 2023 (a total of 10 times).

To further determine whether the candidate root gene *OsIAA8* could improve drought resistance, we conducted a pot experiment. Specifically, the seeds were soaked and germinated, and then seedlings were hydroponically grown for 3 weeks and transplanted into individual round pots (20 cm in diameter, 18 cm in depth) containing 2.5 kg of black soil sourced from Northeast China. There were 12 replicates for each material. The pot experiments were performed outdoors for 60 days, and then the pots were transferred to a greenhouse for drought treatments and phenotyping. Under drought stress (without watering), the soil water content dropped to approximately 15% and was held for 10 days, with the pots weighed every 2 days to ensure this 15% water content. After 10days of drought stress, phenotypic data were acquired in an imaging dark chamber, and image-based phenotyping was conducted to extract phenotype traits such as the total projected area (TPA), green projected area (GPA) and total biomass ratio (TBR). On day 15 post drought stress, all the plants were re-watered, and the rice grains were harvested at maturity.

High-throughput root phenotyping platform

The high-throughput root phenotyping platform is located in Huazhong Agricultural University in Wuhan city, China. The platform is composed of rhizoboxes, frames, rhizobox placement racks, data collection automated guided vehicle (AGV) and an electric extensible shelter (Figure 6a). This platform includes 10 sets of frames, and each frame contains 21 rows of rhizobox placement racks with eight rhizoboxes in each row rack, exhibiting a total throughput of 1680 seedlings (one seedling per rhizobox). The electric extensible shelter can open and close in an east–west direction to provide rain shelter (Figure 6b), enabling the simulation of a natural growth environment, meanwhile meeting drought stress conditions. The rhizobox exhibits a flat rectangular structure (60 cm in height, 30 cm in width and 1.5 cm in thickness). This flat rectangular rhizobox features steel plates on the front, two sides, and bottom, with a transparent glass panel embedded on the back and an open top

(Figure 6c). The rhizoboxes are placed on the placement rack at a 45° angle, with the glass side downwards. This positioning utilizes the geotropic nature of roots, enabling them to adhere to the glass surface for growth. The platform is equipped with an automatic drip irrigation system to ensure a controllable water supply.

The image collection trolley AGV is equipped with a Basler-acA5472 camera (Basler AG, Germany), which is positioned at a 45° angle with the camera's optical axis perpendicular to the glass surface of the rhizobox. A row of light tubes is installed in the rear of the AGV for illumination. The camera can move laterally along the AGV module with four vertical limit sensors between two rhizoboxes. When the camera detects the limit switch during movement, it halts to capture the root images. The AGV moves along a circular track beneath the rhizobox rack. When the sensor of the AGV detects the rhizobox rack, the AGV stops in front of the rhizobox to capture images. The camera captures images at a resolution of 5472 × 3648 pixels, with two rhizoboxes per image and four images per row of the rhizobox rack (Figure 6a). The image acquisition workflow of the platform is shown in Movie S1.

Root phenotype extraction tool (RPT)

In this study, the root phenotype extraction tool RPT was developed using the Qt Library (Summerfield, 2007) and OpenCV (34), and RPT integrated deep learning training and prediction functions for root segmentation. This tool is user-friendly, requiring no installation and it can be directly compiled from the source code, exhibiting the functions of root inpainting and root trait extraction. Users can install CUDA and cuDNN for graphics processing unit (GPU) acceleration (Note S2). The RPT operation procedures are presented in Movie S2. The key functions and algorithm of RPT are as follows.

1. Root segmentation (Figure 7a). The training and evaluation of our developed root segmentation deep learning network EsegFormer and other deep learning models were carried out using the open-source platform PaddleSeg (Liu *et al.*, 2021). To enhance model robustness and expand the dataset, a variety of data augmentation techniques were applied during the training process, including random scaling, cropping, horizontal flipping, blurring, distortion, noise addition and normalization. To accelerate convergence, transfer learning was performed using pretrained models provided by PaddleSeg. The initial learning rate for all models was set at 0.0005 and updated dynamically using a cosine annealing strategy. The models were trained with over 3000 iterations and a batch size of 8. All training and inference processes were executed on a Windows 10 computer equipped with an Intel® Core™ i5-8500 CPU, 16GB of RAM and an NVIDIA GeForce RTX 2080Ti GPU with 11GB of VRAM.
2. Root inpainting. In this study, we applied an inpainting approach based on Generative Adversarial Networks (GANs) to restore invisible root parts or those obscured by soil. We used the original U-Net architecture as the backbone network, integrating the edge attention module (EAM) and the convolutional block attention module (CBAM) to enhance feature extraction capabilities. The composite loss function combines adversarial loss, BCE Loss, Dice Loss and perceptual loss, where BCE and Dice Losses explicitly address the binary classification nature of root pixel restoration (root vs non-root), while perceptual loss ensures semantic consistency. The EAM operates in parallel with the U-Net encoder, effectively capturing fine root details through edge-aware feature refinement. After joint processing by both the encoder and edge attention modules, the feature maps are concatenated and fused via 1 × 1 convolutions. The discriminator with a PatchGAN structure is composed of five convolutional layers, and it outputs the results through a Sigmoid activation function (Figure S3). The root inpainting results are shown in Figure 7b.
3. Trait extraction algorithm. Noise removal is a crucial step in root phenotyping to ensure accurate trait extraction since segmentation errors and background complexity can result in distorted measurements. To address noise and segmentation challenges in rhizobox images, a preprocessing workflow was introduced to refine segmentation results and improve trait extraction accuracy (Figure 7c). Complex backgrounds and intermittent root appearances often cause small noise, edge artefacts and fragmented root segments. To preserve binary image characteristics, the isolated noise points were removed through low-pass filtering and three iterations of 3 × 3 median filtering. The connected component analysis was conducted to extract spatial attributes such as bounding rectangle area, pixel count and centroid coordinates. Noise retained within a 100-pixel boundary during perspective transformation was eliminated. A 7 × 7 dilation operation was applied iteratively to reconnect fragmented roots, and a thresholding step was executed to remove small non-root components. The final binary root images were cleaned by masking the processed images with the original segmentation images to restore the lost root pixels so as to ensure completeness and accuracy.

The trait calculations were implemented using NumPy (33), OpenCV (34) and scikit-image (35) in Python modules. Detailed trait information, including definitions of traits and methods of calculation, is provided in Table S1.

Deep learning datasets for root segmentation

The data used for deep learning training included the image data of rice, cotton, rape and wheat crops planted on the platform. A total of 365 images were randomly selected to train and test the deep learning model. All the images representing individual rhizoboxes were corrected to the same size. The detailed correction method is shown in Figure S2. Training labels were generated using Adobe Photoshop 2021 (Adobe Inc. 2021) image processing software, and the dataset was divided into a training set and a validation set at a ratio of 7:3, with 258 images in the training set and 108 images in the validation set.

Further, label annotation was performed. Specifically, the original image was opened using the annotation software; a new annotation layer was created; the layer transparency was set at about 30%; and the root regions were drawn on the annotation layer using the pencil tool white hard round brush, with red-green-blue (RGB) values set at 255, 255 and 255, respectively. After the annotation of the entire image, the annotation layer transparency was set back to 0%, and the annotation layer was saved separately. Our labelled root image data could be downloaded at the following website: https://drive.google.com/drive/folders/1UJ2XJui8dww-tAPjvh1U72tzFC9Uug9M?usp=drive_link.

The images used for model generalization testing in this study are sourced as follows: Figure 5b (root system image of *Cichorium*

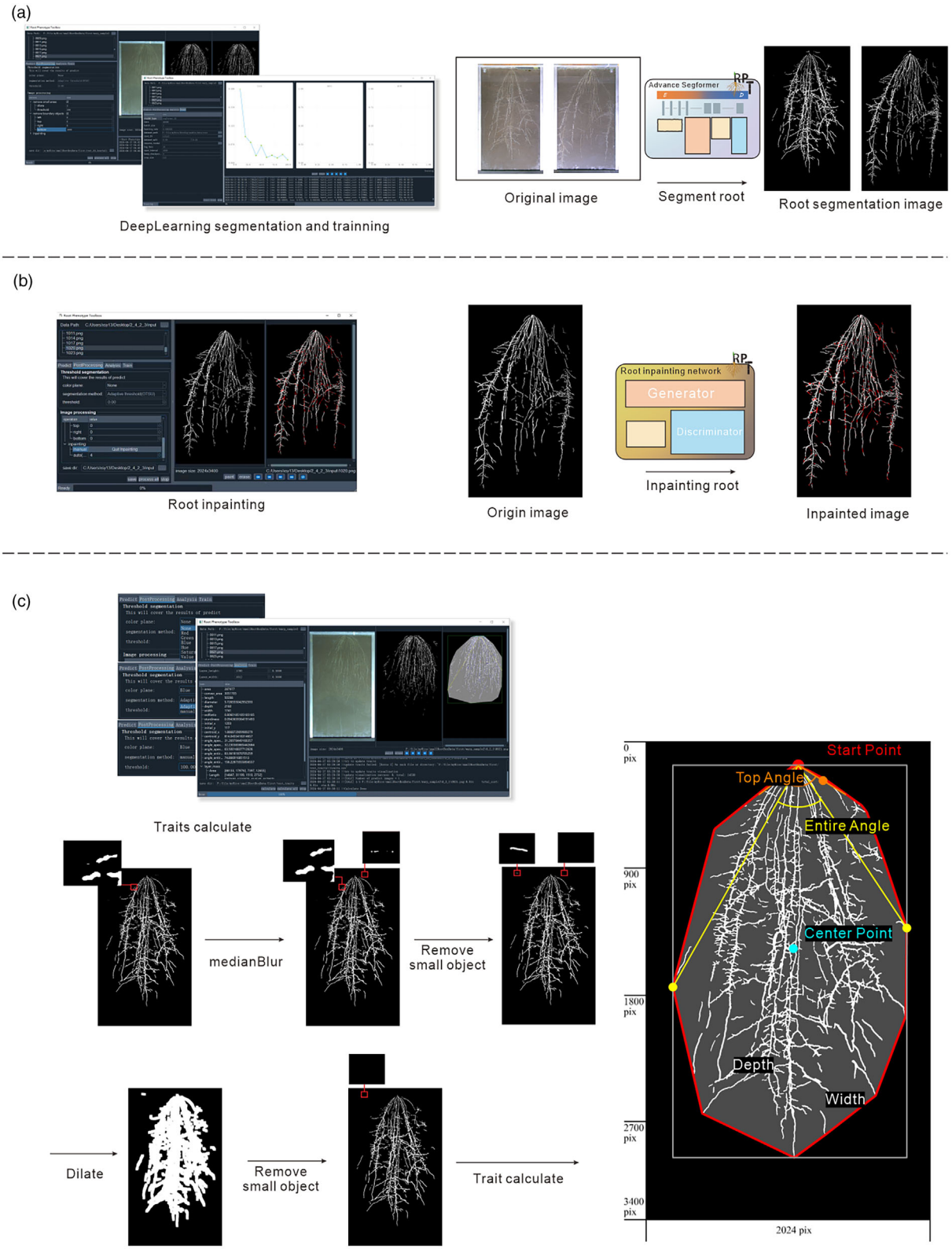

Figure 7 Main functions of the RPT software. (a) Deep learning root segmentation prediction and training. (b) Root inpainting function. (c) Noise removal from binary root images and trait extraction.

intybus line) from the University of Copenhagen (Smith *et al.*, 2020) and Figure 5c (Sesame root system image) from Texas A&M University (Peeples *et al.*, 2023). Additionally, Figure 5d (wheat root system image) comes from the Crop Phenotyping Platform, Henan University. To further validate the performance of our model after fine-tuning, root images from the

large rhizobox phenotyping platform at Huazhong Agricultural University were used.

Deep learning evaluation metrics

The semantic segmentation involves categorizing each pixel in an image into specific classes, typically the foreground or the background. Four evaluation metrics are commonly used to assess the performance of segmentation models, including mean accuracy (mAcc), mean intersection over union (mIoU), mean dice coefficient (mDice) and model total number of parameters. These metrics are derived from the confusion matrix, which classifies pixels into true positives (TP), false positives (FP), false negatives (FN) and true negatives (TN). The background is defined as the negative class, and the root as the positive class. Consistency between the model's predictions and the ground truth can be determined by the confusion matrix analysis.

Mean accuracy (mAcc) refers to the average of the pixel-wise accuracy across all test samples. It reflects the ratio of correctly predicted pixels to the total number of pixels, and it is calculated according to the following formula:

$$\text{Accuracy} = \frac{\text{TP} + \text{TN}}{TP + \text{TN} + \text{FP} + \text{FN}}$$

$$\text{mAcc} = \frac{1}{N}\sum_{i=1}^{N} \text{Accuracy}_i$$

where N is the number of tested samples; Accuracy_i is the accuracy score of the i-th tested sample.

Mean intersection over union (mIoU) is the average of the intersection over union (IoU) scores for all tested samples. It is used to evaluate segmentation performance by measuring the overlapping degree between the predicted regions and ground truth regions. It is calculated according to the following formula.

$$\text{IoU} = \frac{\text{TP}}{\text{TP} + \text{FP} + \text{FN}}$$

$$\text{mIoU} = \frac{1}{N}\sum_{i=1}^{N} \text{IoU}_i$$

where N is the number of tested samples; IoU_i is the IoU score for the i-th tested sample.

Mean dice coefficient (mDice) is the average of the dice coefficients across all tested samples. It measures the similarity between the predicted region and ground truth region. The higher the value, the better the performance. Its calculation formula is as follows:

$$\text{Dice} = \frac{2\text{TP}}{2\text{TP} + \text{FP} + \text{FN}}$$

$$\text{mDice} = \frac{1}{N}\sum_{i=1}^{N} \text{Dice}_i$$

where N is the number of tested samples; and Dice_i is the dice coefficient of the i-th tested sample.

Trait calculation accuracy evaluation indicators

To evaluate the trait calculation accuracy of our experimental method, true values of root traits were extracted using open-source software RhizoVision Explorer (Seethepalli *et al.*, 2021), which has been validated to have high accuracy on copper wire image sets and simulated root data. The tested samples were the same as those in the deep learning validation set. R^2, mean absolute percentage error (MAPE), and root mean square error (RMSE) were used for evaluating trait calculation accuracy.

$$R^2 = \frac{\text{SSR}}{\text{SST}} = \frac{\sum_i (\hat{y}_i - \bar{y})^2}{\sum_i (y_i - \bar{y})^2}$$

where n is the number of samples; $\hat{y}_i$ are the predicted values of the ith sample; y_i are the true values of the ith sample; $\bar{y}$ is the mean of the true values; SSR is the sum of squares of the regression; and SST is the total sum of squares.

$$\text{MAPE} = \frac{1}{n}\sum_i \left|\frac{y_i - x_i}{x_i}\right| \times 100\%$$

where n is the number of samples; x_i is the true value of the ith sample, and y_i is the predicted value of the ith sample.

$$\text{RMSE} = \sqrt{\frac{\sum_i (y_i - x_i)^2}{n}}$$

where y_i are the predicted values of the ith sample, x_i are the true values of the ith sample, and n is the number of samples.

Acknowledgements

This work was supported by the National key Research and Development plan (2022YFD2002304), National Natural Science Foundation of China (U21A20205), Key Agricultural Technology Research Project in Hubei Province (HBNYHXGG2023-9) and Fundamental Research Funds for the Central Universities (2662024ZKPY003).

Author contributions

W.Y. and Q.L. designed the research. J.S. and S.X. conceived the project and supervised the study. J.S. and S.X. performed the experiments and analysed the data. J.S., S.X. and X.W. wrote the manuscript. W.L., J.S. and S.X. designed and built the hardware. X.W., J.W. and Y.C. provided the materials and supported the data. W.Y., Q.L. and Y.C. provided constructive suggestions and revised the manuscript. All authors read and approved the final manuscript.

Conflict of interest

The authors declare no competing financial interests.

Data availability

The root phenotypic data used in this study, including pre- and post-inpainting data, are presented in Table S2. The source code for RPT can be downloaded from https://github.com/shijiawei124/RPT.git, and the root training labels in this study are available on Google Drive https://drive.google.com/drive/folders/1UJ2XJui8dww-tAPjvh1U72tzFC9Uug9M?usp=drive_link. Data and research materials can be obtained by contacting the corresponding authors.

References

Ahmadi, N., Audebert, A., Bennett, M.J., Bishopp, A., de Oliveira, A.C., Courtois, B., Diedhiou, A. *et al*. (2014) The roots of future rice harvests. *Rice.* **7**, 29.

Arsenault, J.-L., Poulcur, S., Messier, C. and Guay, R. (1995) WinRHlZO™, a root-measuring system with a unique overlap correction method. *Hort Science.* **30**, 906D–906D.

Atkinson, J.A., Pound, M.P., Bennett, M.J. and Wells, D.M. (2019) Uncovering the hidden half of plants using new advances in root phenotyping. *Curr. Opin. Biotechnol.* **55**, 1–8.

Badrinarayanan, V., Kendall, A. and Cipolla, R. (2017) Segnet: A deep convolutional encoder-decoder architecture for image segmentation. *IEEE Trans. Pattern Anal. Mach. Intell.* **39**, 2481–2495.

Baoxiang, W., Yan, L., Yifeng, W., Jingfang, L., Zhiguang, S., Ming, C., Yungao, X. *et al*. (2021) OsbZIP72 Is Involved in Transcriptional Gene-Regulation Pathway of Abscisic Acid Signal Transduction by Activating Rice High-Affinity Potassium Transporter OsHKT1;1. *Ric. Sci.* **28**, 257–267.

Bolger, M., Schwacke, R., Gundlach, H., Schmutzer, T., Chen, J., Arend, D., Oppermann, M. *et al*. (2017) From plant genomes to phenotypes. *J. Biotechnol.* **261**, 46–52.

Bontpart, T., Concha, C., Giuffrida, M.V., Robertson, I., Admkie, K., Degefu, T., Girma, N. *et al*. (2020) Affordable and robust phenotyping framework to analyse root system architecture of soil-grown plants. *Plant J.* **103**, 2330–2343.

Bosilj, P., Aptoula, E., Duckett, T. and Cielniak, G. (2020) Transfer learning between crop types for semantic segmentation of crops versus weeds in precision agriculture. *J. Field Robot.* **37**, 7–19.

Le Bot, J., Serra, V., Fabre, J., Draye, X., Adamowicz, S. and Pagès, L. (2010) DART: a software to analyse root system architecture and development from captured images. *Plant and Soil* **326**, 261–273.

Chen, Y.L., Dunbabin, V.M., Diggle, A.J., Siddique, K.H.M. and Rengel, Z. (2011) Development of a novel semi-hydroponic phenotyping system for studying root architecture. *Funct. Plant Biol.* **38**, 355–363.

Chen, X., Wang, Y., Lv, B., Li, J., Luo, L., Lu, S., Zhang, X. *et al*. (2014) The NAC family transcription factor OsNAP confers abiotic stress response through the ABA pathway. *Plant Cell Physiol.* **55**, 604–619.

Chen, L.-C., Zhu, Y., Papandreou, G., Schroff, F. and Adam, H. (2018) Encoder-decoder with atrous separable convolution for semantic image segmentation. In *Proceedings of the European conference on computer vision (ECCV)*, pp. 801–818. Berlin, Germany: Springer.

Cobb, J.N., DeClerck, G., Greenberg, A., Clark, R. and McCouch, S. (2013) Next-generation phenotyping: requirements and strategies for enhancing our understanding of genotype–phenotype relationships and its relevance to crop improvement. *Theor. Appl. Genet.* **126**, 867–887.

van Dusschoten, D., Metzner, R., Kochs, J., Postma, J.A., Pflugfelder, D., Bühler, J., Schurr, U. *et al*. (2016) Quantitative 3D Analysis of Plant Roots Growing in Soil Using Magnetic Resonance Imaging. *Plant Physiol.* **170**, 1176–1188.

Haling, R.E., Tighe, M.K., Flavel, R.J. and Young, I.M. (2013) Application of X-ray computed tomography to quantify fresh root decomposition in situ. *Plant and Soil* **372**, 619–627.

Jeong, J.S., Kim, Y.S., Redillas, M.C., Jang, G., Jung, H., Bang, S.W., Choi, Y.D. *et al*. (2013) OsNAC5 overexpression enlarges root diameter in rice plants leading to enhanced drought tolerance and increased grain yield in the field. *Plant Biotechnol. J.* **11**, 101–114.

Kamilaris, A. and Prenafeta-Boldú, F.X. (2018) Deep learning in agriculture: A survey. *Comput. Electron. Agr.* **147**, 70–90.

Li, L., Li, N., Song, S.F., Li, Y.X., Xia, X.J., Fu, X.Q., Chen, G.H. *et al*. (2014) Cloning and characterization of the drought-resistance OsRCI2-5 gene in rice (*Oryza sativa* L.). *Genet. Mol. Res.* **13**, 4022–4035.

Li, X., Guo, Z., Lv, Y., Cen, X., Ding, X., Wu, H., Li, X. *et al*. (2017) Genetic control of the root system in rice under normal and drought stress conditions by genome-wide association study. *PLoS Genet.* **13**, e1006889.

Li, A., Zhu, L., Xu, W., Liu, L. and Teng, G. (2022) Recent advances in methods for in situ root phenotyping. *PeerJ* **10**, e13638.

Liu, W.Y., Wang, M.M., Huang, J., Tang, H.J., Lan, H.X. and Zhang, H.S. (2009) The OsDHODH1 gene is involved in salt and drought tolerance in rice. *J. Integr. Plant Biol.* **51**, 825–833.

Liu, Y., Chu, L., Chen, G., Wu, Z., Chen, Z., Lai, B. and Hao, Y. (2021) *Paddleseg: A high-efficient development toolkit for image segmentation*. arXiv preprint arXiv:2101.06175.

Luo, L., Mei, H., Yu, X., Xia, H., Chen, L., Liu, H., Zhang, A. *et al*. (2019) Water-saving and drought-resistance rice: from the concept to practice and theory. *Mol. Breed.* **39**, 145.

Luo, Z., Yang, W., Yuan, Y., Gou, R. and Li, X. (2024) Semantic segmentation of agricultural images: A survey. *Inf. Process. Agric.* **11**, 172–186.

Matsuda, S., Takano, S., Sato, M., Furukawa, K., Nagasawa, H., Yoshikawa, S., Kasuga, J. *et al*. (2016) Rice Stomatal Closure Requires Guard Cell Plasma Membrane ATP-Binding Cassette Transporter RCN1/OsABCG5. *Mol. Plant* **9**, 417–427.

Meng, F., Xiang, D., Zhu, J., Li, Y. and Mao, C. (2019) Molecular Mechanisms of Root Development in Rice. *Rice.* **12**(1), 1.

Metzner, R., Eggert, A., Dusschoten, D., Pflugfelder, D., Gerth, S., Schurr, U., Uhlmann, N. *et al*. (2015) Direct comparison of MRI and X-ray CT technologies for 3D imaging of root systems in soil: potential and challenges for root trait quantification. *Plant Methods* **11**, 17.

Milioto, A., Lottes, P. and Stachniss, C. (2018) Real-Time Semantic Segmentation of Crop and Weed for Precision Agriculture Robots Leveraging Background Knowledge in CNNs. In *2018 IEEE International Conference on Robotics and Automation (ICRA)*, pp. 2229–2235. Piscataway, NJ: IEEE.

Mu, P. (2003) QTL mapping of the root traits and their correlation analysis with drought resistance using DH lines from paddy and upland rice cross. *Chin. Sci. Bull.* **48**, 2718–2724.

Mukhopadhyay, R., Sarkar, B., Jat, H.S., Sharma, P.C. and Bolan, N.S. (2021) Soil salinity under climate change: Challenges for sustainable agriculture and food security. *J. Environ. Manage.* **280**, 111736.

Nagel, K.A., Putz, A., Gilmer, F., Heinz, K., Fischbach, A., Pfeifer, J., Faget, M. *et al*. (2012) GROWSCREEN-Rhizo is a novel phenotyping robot enabling simultaneous measurements of root and shoot growth for plants grown in soil-filled rhizotrons. *Funct. Plant Biol.* **39**, 891–904.

Nagel, K.A., Lenz, H., Kastenholz, B., Gilmer, F., Averesch, A., Putz, A., Heinz, K. *et al*. (2020) The platform GrowScreen-Agar enables identification of phenotypic diversity in root and shoot growth traits of agar grown plants. *Plant Methods* **16**, 89.

Peeples, J., Xu, W., Gloaguen, R., Rowland, D., Zare, A. and Brym, Z. (2023) Spatial and texture analysis of root system distribution with earth mover's distance (STARSEED). *Plant Methods* **19**, 2.

Pierret, A., Gonkhamdee, S., Jourdan, C. and Maeght, J.-L. (2013) IJ_Rhizo: an open-source software to measure scanned images of root samples. *Plant and Soil* **373**, 531–539.

Pound, M.P., French, A.P., Atkinson, J.A., Wells, D.M., Bennett, M.J. and Pridmore, T. (2013) RootNav: Navigating Images of Complex Root Architectures. *Plant Physiol.* **162**, 1802–1814.

Rellán-Álvarez, R., Lobet, G., Lindner, H., Pradier, P.-L., Sebastian, J., Yee, M.-C., Geng, Y. *et al*. (2015) GLO-Roots: an imaging platform enabling multidimensional characterization of soil-grown root systems. *Elife* **4**, e07597.

Ronneberger, O., Fischer, P. and Brox, T. (2015) U-net: Convolutional networks for biomedical image segmentation. In *Medical image computing and computer-assisted intervention–MICCAI 2015: 18th international conference, Munich, Germany, October 5-9, 2015, proceedings, part III 18 pp*, pp. 234–241. Berlin, Germany: Springer.

Sahid, S., Roy, C., shee, D., Shee, R., Datta, R. and Paul, S. (2023) ZFP37, C3H, NAC94, and bHLH148 transcription factors regulate cultivar-specific drought response by modulating r40C1 gene expression in rice. *Environ. Exp. Bot.* **214**, 105480.

Santosh Kumar, V.V., Yadav, S.K., Verma, R.K., Shrivastava, S., Ghimire, O., Pushkar, S., Rao, M.V. *et al*. (2021) The abscisic acid receptor OsPYL6 confers drought tolerance to indica rice through dehydration avoidance and tolerance mechanisms. *J. Exp. Bot.* **72**, 1411–1431.

Santos-Medellín, C., Liechty, Z., Edwards, J., Nguyen, B., Huang, B., Weimer, B.C. and Sundaresan, V. (2021) Prolonged drought imparts lasting compositional changes to the rice root microbiome. *Nat. Plants.* **7**, 1065–1077.

Seethepalli, A., Dhakal, K., Griffiths, M., Guo, H., Freschet, G.T. and York, L.M. (2021) RhizoVision Explorer: open-source software for root image analysis and measurement standardization. *AoB PLANTS.* **13**, plab056.

Selvaraj, M.G., Montoya-P, M.E., Atanbori, J., French, A.P. and Pridmore, T. (2019) A low-cost aeroponic phenotyping system for storage root development: unravelling the below-ground secrets of cassava (Manihot esculenta). *Plant Methods* **15**, 131.

Shi, L., Guo, M., Ye, N., Liu, Y., Liu, R., Xia, Y., Cui, S. *et al*. (2015) Reduced ABA Accumulation in the Root System is Caused by ABA Exudation in Upland Rice (Oryza sativa L. var. Gaoshan1) and this Enhanced Drought Adaptation. *Plant Cell Physiol.* **56**, 951–964.

Singh, K.K. and Ghosh, S. (2013) Regulation of glutamine synthetase isoforms in two differentially drought-tolerant rice (Oryza sativa L.) cultivars under water deficit conditions. *Plant Cell Rep.* **32**, 183–193.

Smith, A.G., Petersen, J., Selvan, R. and Rasmussen, C.R. (2020) Segmentation of roots in soil with U-Net. *Plant Methods* **16**, 13.

Summerfield, M. (2007) *Rapid GUI Programming with Python and Qt: The Definitive Guide to PyQt Programming*. London: Pearson Education.

Tamiru, M., Undan, J.R., Takagi, H., Abe, A., Yoshida, K., Undan, J.Q., Natsume, S. *et al*. (2015) A cytochrome P450, OsDSS1, is involved in growth and drought stress responses in rice (Oryza sativa L.). *Plant Mol. Biol.* **88**, 85–99.

Trachsel, S., Kaeppler, S.M., Brown, K.M. and Lynch, J.P. (2011) Shovelomics: high throughput phenotyping of maize (Zea mays L.) root architecture in the field. *Plant and Soil* **341**, 75–87.

Uga, Y., Okuno, K. and Yano, M. (2011) Dro1, a major QTL involved in deep rooting of rice under upland field conditions. *J. Exp. Bot.* **62**, 2485–2494.

Vogel, E., Donat, M.G., Alexander, L.V., Meinshausen, M., Ray, D.K., Karoly, D., Meinshausen, N. *et al*. (2019) The effects of climate extremes on global agricultural yields. *Environ. Res. Lett.* **14**, 054010.

Xiong, L. and Yang, Y. (2003) Disease resistance and abiotic stress tolerance in rice are inversely modulated by an abscisic acid-inducible mitogen-activated protein kinase. *Plant Cell* **15**, 745–759.

Yang, W., Feng, H., Zhang, X., Zhang, J., Doonan, J.H., Batchelor, W.D., Xiong, L. *et al*. (2020) Crop Phenomics and High-Throughput Phenotyping: Past Decades, Current Challenges, and Future Perspectives. *Mol. Plant* **13**, 187–214.

Zhang, Q. (2007) Strategies for developing Green Super Rice. *Proc. Natl. Acad. Sci.* **104**, 16402–16409.

Zhang, D., Yang, H., Wang, X., Qiu, Y., Tian, L., Qi, X. and Qu, L.Q. (2020) Cytochrome P450 family member CYP96B5 hydroxylates alkanes to primary alcohols and is involved in rice leaf cuticular wax synthesis. *New Phytol.* **225**, 2094–2107.

Zhao, H., Shi, J., Qi, X., Wang, X. and Jia, J. (2017) Pyramid Scene Parsing Network. In *Proceedings of the IEEE conference on computer vision and pattern recognition*, pp. 2881–2890. Piscataway, NJ: IEEE.

Zheng, C., Zhou, J., Zhang, F., Yin, J., Zhou, G., Li, Y., Chen, F. *et al*. (2020) OsABAR1, a novel GRAM domain-containing protein, confers drought and salt tolerance via an ABA-dependent pathway in rice. *Plant Physiol. Biochem.* **152**, 138–146.

Supporting information

Additional supporting information may be found online in the Supporting Information section at the end of the article.

Figure S1 RPT architecture.
Figure S2 Segmentation correction algorithm for glass surface.
Figure S3 Root inpainting network architecture.
Table S1 Root traits and their definitions.
Table S2 Raw data of extracted root phenotypes before and after inpainting.
Table S3 Genotypic data of recombinant inbred line (RIL) population.
Table S4 QTL mapping results and co-localization results before and after root inpainting and candidate QTLs.
Table S5 Raw phenotypic data of rhizobox and Pot experiments on IAA8-overexpressing (IAA8OE) and Nip materials.
Movie S1 Real scene and workflow of a high-throughput root phenotyping platform.
Movie S2 Operation of RPT.
Note S1 Detailed information of all the supplemental figures.
Note S2 Environment configuration.